RSC Advances

PAPER

View Article Online
View Journal | View Issue

Cite this: *RSC Adv.*, 2022, **12**, 36126

Room temperature dilute magnetic semiconductor response in (Gd, Co) co-doped ZnO for efficient spintronics applications

Rajwali Khan, *[ab] Ihab Shigidi, [c] Sattam Al Otaibi,[d] Khaled Althubeiti, [e] Sherzod Shukhratovich Abdullaev,†[f] Nasir Rahman, [b] Mohammad sohail,[b] Alamzeb Khan,[g] Shahid Iqbal,[h] Tommaso Del Rosso,[i] Quaid Zaman [j] and Aurangzeb Khan[k]

The co-precipitation approach was utilized to experimentally synthesize ZnO, $Zn_{0.96}Gd_{0.04}O$ and $Zn_{0.96-x}Gd_{0.04}Co_xO$ (Co = 0, 0.01, 0.03, 0.04) diluted magnetic semiconductor nanotubes. The influence of gadolinium and cobalt doping on the microstructure, morphology, and optical characteristics of ZnO was investigated, and the Gd doping and Co co-doping of the host ZnO was verified by XRD and EDX. The structural investigation revealed that the addition of gadolinium and cobalt to ZnO reduced crystallinity while maintaining the preferred orientation. The SEM study uncovered that the gadolinium and cobalt dopants did not affect the morphology of the produced nanotubes, which is further confirmed through TEM. In the UV-vis spectra, no defect-related absorption peaks were found. By raising the co-doping content, the crystalline phase of the doped samples was enhanced. It was discovered that the dielectric response and the a.c. electrical conductivity display a significant dependent relationship. With the decreasing frequency and increasing Co co-dopant concentration, the ε_r and ε'' values decreased. It was also discovered that the ε_r, ε'', and a.c. electrical conductivity increased when doping was present. Above room temperature, co-doped ZnO nanotubes exhibited ferromagnetic properties. The ferromagnetic behaviour increased as Gd (0.03) doping increased. Increasing the Co content decreased the ferromagnetic behaviour. It was observed that $Zn_{0.96-x}Gd_{0.04}Co_xO$ (x = 0.03) nanotubes exhibit superior electrical conductivity, magnetic and dielectric characteristics compared to pure ZnO. This high ferromagnetism is typically a result of a magnetic semiconductor that has been diluted. In addition, these nanoparticles are utilized to design spintronic-based applications in the form of thin-films.

Received 20th October 2022
Accepted 5th December 2022

DOI: 10.1039/d2ra06637h

rsc.li/rsc-advances

1. Introduction

The research work on oxide semiconductors doped with transition metals (TMs)[1–8] has attracted many researchers, focusing on diluted magnetic semiconductor (DMS)-based compounds for spintronics-related applications. The discovery of ferromagnetism (FM) in $Ga_{1-x}Mn_xAs$ allowed much progress in DMS for electronic devices related to spin (spintronics)[9] including the quantum Hall effect, single electronic charging, resistive switching devices, and semiconductor lasers. Moreover, a large number of technological applications such as photonics, biosensors, nanoelectronics, light-emitting devices (LED), optoelectronics, and spin-based devices have been commercialized.[10–15] These devices are interesting in that there is the possibility of realizing a DMS Curie temperature (T_C) above room temperature ferromagnetism (RTFM). Many previous studies[13,16–18] used TMs doped with II–VI and III–V semiconductors to create a FM phase in the host ZnO. This behavior is welcome in many real-life applications and has caused some controversy about the origin of FM. Many materials with non-magnetic ions have

[a]Department of Physics, Zhejiang University, Hangzhou, China. E-mail: khan_phy@foxmail.com; rajwalipak@zju.edu.pk
[b]Department of Physics, University of Lakki Marwat, 28420 KP, Pakistan
[c]Chemical Engineering Department, King Khalid University, P.O. Box 395, Abha 61411, Saudi Arabia
[d]Department of Electrical Engineering, College of Engineering, Taif University, P.O. Box 110, Taif 21944, Saudia Arabia
[e]Department of Chemistry, College of Science, Taif University, P.O. Box 110, Taif 21944, Saudia Arabia
[f]Andijan Machine-Building Institute, Andijan, Uzbekistan
[g]Department of Pediatrics, Yale School of Medicine, Yale University, New Haven, CT, 06511, USA
[h]Department of Physics, Albion College, Albion, Michigan, 49224, USA
[i]Department of Physics, Pontifícia Universidade Católica do Rio de Janeiro, Rua Marques de São Vicente, 22451-900, Rio de Janeiro, Brazil
[j]Department of Physics, University of Buner, Pakistan
[k]Department of Physics, Abdul Wali Khan University, KP, Pakistan
† CEO of the Company of Editory, Tashkent, Uzbekistan.

exhibited unexpected FM behaviour[11,18,19] provoking interest to further research the RTFM of these structures. This is a new study for spin-based electronics. Spin-based electronics can be used for devices specially RRAM and hard drives.

DMS in II–VI semiconductor materials emanates from the introduction of TMs with 3d electrons in the lattice.[13] Among these, Co-doped ZnO has interesting properties.[7,20] Because cobalt (Co) is one of the most soluble transition metal ions in ZnO. In addition, it has the same ionic radius as the zinc (Zn) ion, which is favorable for doping at the Zn^{2+} site. ZnO can grow into many different shapes, such as spheres and dumbbells, rods, nanonails, hollow nanospheres, rods that look like pyramids or laths, flowers, and nanowires. For DMS to work well in industrial settings, its size and shape are very important. Nanostructures can change shape from top to bottom by doping, but it's hard to control the shape. The shape, size, structure, and optical properties are all affected by the amount of doping, how long it is heated, and how hot it grows. The level of TM ions substitution determines the ferromagnetic behaviour. The first RTFM in Mn-doped ZnO nanoparticles was recently reported by Hao *et al.*[21] Oshio *et al.*[22] later studied leakage current in the epitaxial film using this material. Recently, the behaviour of semiconductor quantum dots and Co–ZnO nanoparticles RTFM has been studied.[23] It was demonstrated that Co doping caused defects and oxygen vacancies. This was demonstrated by an increase in luminescence intensity in the visible region of the PL spectra, indicating that the defects and vacancies were caused by Co doping. Controlling defects, in addition to shape and size, is critical for the application of ZnO because imperfections can alter the material's properties. The RTFM properties in Fe-doped ZnO nanoparticles were also reported by Xu *et al.*[24] The TMs-ZnO dielectric and electrical properties are also required in high-frequency electronic devices.[25–27] Despite many experimental and theoretical reports on ZnO, the work on doped TMs is still controversial.

In this paper, we report the synthesis of ZnO, $Zn_{0.96}Gd_{0.04}O$ and $Zn_{0.96-x}Gd_{0.04}Co_xO$ (Co = 0, 0.01, 0.03, 0.04) nanotubes (NTs) by co-precipitation method with varying concentrations of Co while keeping the Gd content at a fixed concentration. The changing in the concentration of Co altered the crystallinity and indicated a hindrance in the recombination rate of photoinduced electron–hole pairs in ZnO. This enhanced dielectric and magnetic response of zinc NTs.

2. Materials and methods

2.1 Chemicals

The reagents, zinc chloride [$ZnCl_2 \cdot 6H_2O$], gadolinium chloride [$GdCl_3 \cdot 6H_2O$], and cobalt chloride [$CoCl_2 \cdot 4H_2O$] were purchased from Alfa-Aesar and used as received.

2.2 Sample preparation

The (Gd, Co) co-doped ZnO specimens were produced in fewer mounts by using the co-precipitation method. The procedure was to dissolve zinc chloride [$ZnCl_2 \cdot 6H_2O$], in 40 ml pure water before the dropwise addition of 24 ml of aqueous ammonia solution (1.7 M) and urea with strong stirring whilst pH is controlled between 1.0 and 10.2.[28,29] Finally, brownish-type powder was accumulated by washing and centrifugation after the reaction. They were then dried at 70 °C for 28 h before annealing at 500 °C for 3 h in a furnace. For the Gd and Co co-doped specimens, zinc, gadolinium, and cobalt acetate were slowly dripped whilst stirring before separating the precipitates.

2.3 Instruments

The Cu Kα radiation ($\lambda = 1.5406$ Å) from XRD was employed for structural characterization. The High Score Plus software was used for the Rietveld refinements to determine the specimen's lattice parameters and volumes. A field emission scanning electron microscope was utilized to examine the particle shapes (FE-SEM). Transmission electron microscopy was utilized to determine the nature of the particles. The UV-vis spectrometer was utilized to examine the optical absorption spectrum. In the frequency range of 40 Hz to 5 MHz, dielectric properties and electrical conductivity were measured using the impedance analyzer from the frequency range of 40 Hz to 1 MHz. A Quantum Design superconducting quantum interface device (SQUID) was used to measure diluted magnetic semiconductor properties.

3. Results and discussions

3.1 Structural properties

The XRD result of ZnO, $Zn_{0.96}Gd_{0.04}O$ and $Zn_{0.96-x}Gd_{0.04}Co_xO$ (Co = 0, 0.01, 0.03, 0.04) NTs, are displayed in Fig. 1. In all the specimens, no impurities phase was detected and crystallized with the hexagonal structure (wurtzite-type $P6_3mc$ space group). All the lattice constants of $a = 3.2497$ Å, $c = 5.1974$ Å and $a = 3.2457$ Å, $c = 5.1914$ Å were acquired by Rietveld refinement software along with weighted profile factor ($R_{WP} = 9.38\%$, 9.37 and the goodness-of-fit $\chi^2 = 2.571$, 2.581) for the pure ZnO and $Zn_{0.96}Gd_{0.04}O$ as shown in Fig. 1(a) and (b). The unit cell volume for pure ZnO is $V = 47.45$ Å^3 and it is decreased to $V = 47.40$ Å^3 for $Zn_{0.96}Gd_{0.04}O$ specimen (see Fig. 1(b)). For $Zn_{0.93}Gd_{0.04}Co_{0.03}O$, the unit cell volume increased to $V = 47.28$ Å^3, which is higher when compared to pure and $Zn_{0.96}Gd_{0.04}O$. Also, the internal parameter u, which is the length of the bond along the c-axis, is not the same as the value for the ideal wurtzite structure (0.375), as expected for real crystals. Also, the internal parameter goes up as x goes up (as mentioned in Table 1) without keeping an inverse correlation with the c/a ratio, as commonly reported for ZnO.[30] It is anticipated since the ionic radius of Gd^{3+} (94 Å), and Co^{2+} (0.65 Å) are larger than that of Zn^{2+} (0.60 Å). This behaviour can be explained by the fact that Gd^{3+} and Co^{2+} ions replace Zn^{2+} ions in the structure of wurtzite. This is because gadolinium and cobalt ions have larger ionic radii and less electronegativity than zinc ions.[1,23,26] Also, the XRD results support the idea that Gd^{3+} and Co^{2+} ions were put into the wurtzite structure, likely replacing Zn ions. This caused the wurtzite unit cell to change shape. Also, the XRD patterns reveal that the Gd (fixed) and Co co-dopants in ZnO

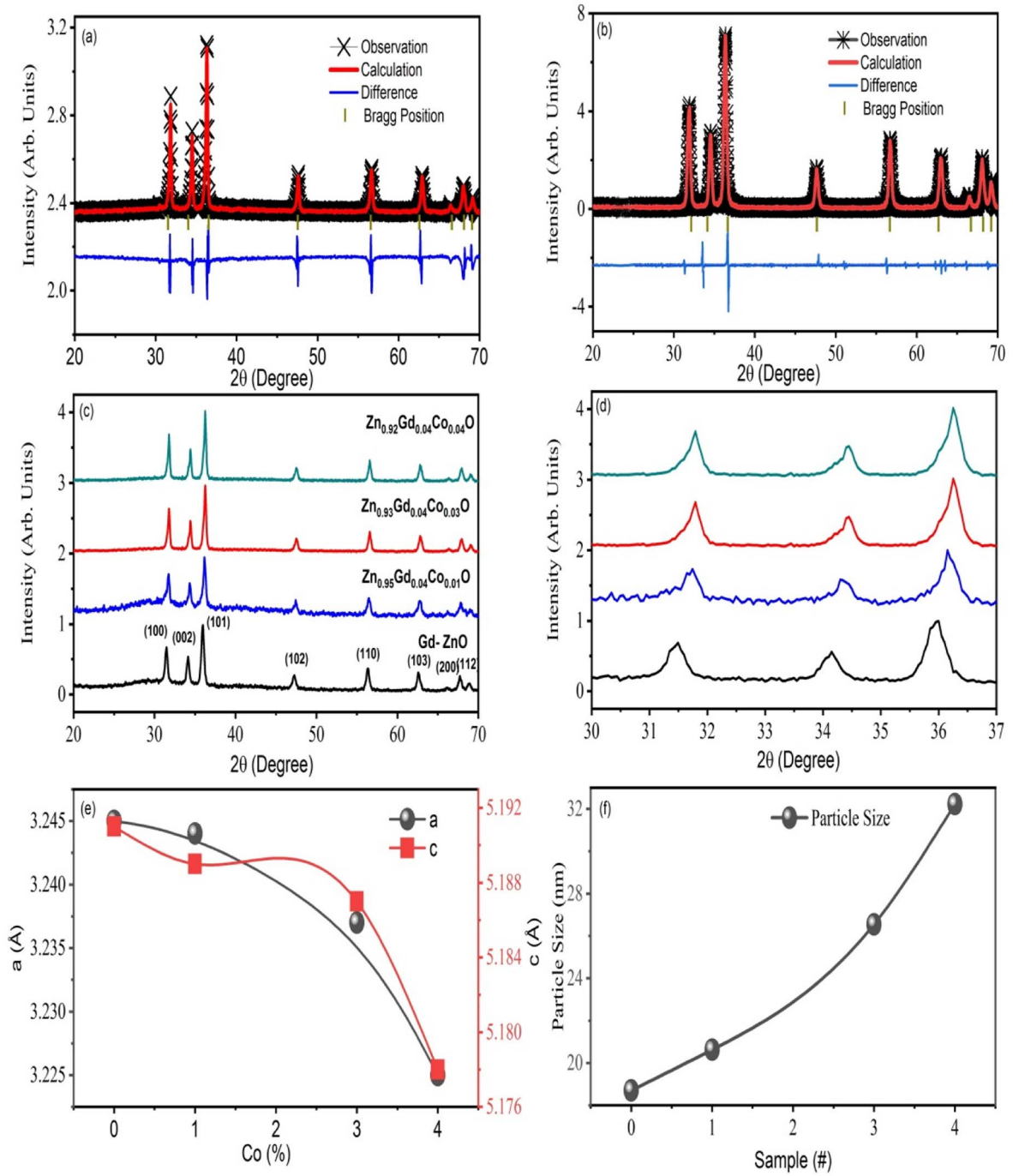

Fig. 1 (a) and (b) The Rietveld refinement of ZnO and $Zn_{0.96}Gd_{0.04}O$ (c) XRD for all the samples. (d) The peak shifting with different doping (e) lattice parameters calculated from XRDs, and (f) the particle size of single doped and $Zn_{0.96-x}Gd_{0.04}Co_xO$ (Co = 0, 0.01, 0.03, 0.04) samples.

increase their concentrations, the peaks shifted at a lower angle, as displayed in Fig. 1(b). It is recommended that specimens are transferred to a disordered form as a result of Gd and Co doping.

The XRD peaks broadening were used for the Scherrer formula to determine the crystallite size of specimens,[27,31] and it was found that size decreased with an increase in Co content from 0 to 4%. Such a decrease can be attributed to grain growth inhibition caused by the presence of Gd and Co in ZnO. This shows that the presence Co in high amounts does not only provide O_2 vacancies to smooth densification to support and inhibits grain development. However, grain boundary segregation in highly doped specimens causes a reduction in particle size. The decrease in lattice parameter with a higher in Co content is because of the lower ionic radius of Co (70 pm) when compared to Zn (74 pm) ions. Table 1 summarizes the calculated X-ray density, grains size, lattice parameters, rain size, and *V*.

The compositions (wt%) of Zn, O, Gd and Co obtained are given by the EDX spectra in Fig. 2(a)–(c). As anticipated, Zn and

Table 1 The variation of structure parameters was calculated from ZnO and $Zn_{0.96-x}Gd_{0.04}Co_xO$ (Co = 0, 0.01, 0.03, 0.04) samples

Sample	*hkl*	*d*-Spacing (Å)	2θ (°)	Grain size (nm)	Lattice constant		*c*/*a*	*u*	Unite cell volume (Å^3)
					a (Å)	*c* (Å)			
ZnO	100	2.7973	31.832	14.34	3.2497	5.1874	1.596	0.388	47.45
	002	2.5972	34.423	13.11	—	—			—
	101	2.4704	36.344	11.45	—	—			—
$Zn_{0.96}Gd_{0.04}O$	100	2.8079	31.847	13.54	3.2457	5.1914	1.599	0.392	47.40
	002	2.5973	34.645	13.61	—	—			—
	101	2.4715	36.465	12.34	—	—			—
$Zn_{0.95}Gd_{0.04}Co_{0.01}O$	100	2.8082	31.902	12.32	3.244	5.189	1.599	0.395	47.37
	002	2.5976	34.670	13.35	—	—			—
	101	2.4719	36.490	14.01	—	—			—
$Zn_{0.93}Gd_{0.04}Co_{0.03}O$	100	2.8085	36.498	14.75	3.237	5.187	1.602	0.399	47.28
	002	2.5980	34.689	15.54	—	—			—
	101	2.4721	36.512	16.4	—	—			—
$Zn_{0.92}Gd_{0.04}Co_{0.04}O$	100	2.8088	36.459		3.225	5.178	1.605	0.401	47.21
	002	2.5984	34.692						
	101	2.4727	36.534						

O are the predominant chemical components in pure ZnO, but Gd and Co co-doped ZnO specimens exhibit Gd and Co peaks. It was discovered that the weight percent of doped TMs was close to the prescribed quantity used for sample preparation as displayed in the inset of Fig. 2(a)–(c). Fig. 2(a)–(c) displays the morphology and elemental analysis of pure, 3 and 4 wt% Gd and Co co-doped ZnO examined by SEM analysis. These results indicate that the NTs have same morphology with hexagonal wurtzite structure. The form of the samples tube-like structure with increasing aggregation as Gd and Co content increases.

The transmission electron microscopy (TEM) images of ZnO, $Zn_{0.93}Gd_{0.04}Co_{0.03}O$, and $Zn_{0.92}Gd_{0.04}Co_{0.04}O$ NTs are displayed in Fig. 3(a)–(c). The TEM images for ZnO, $Zn_{0.93}Gd_{0.04}Co_{0.03}O$ and $Zn_{0.92}Gd_{0.04}Co_{0.04}O$ NTs displayed almost tube-like shaped with a uniform distribution. The TEM study indicates that the mean tube size for pure ZnO is approximately 15 nm, 17 for $Zn_{0.93}Gd_{0.04}Co_{0.03}O$ and 19 nm for $Zn_{0.92}Gd_{0.04}Co_{0.04}O$. The co-doping with Gd and Co enhances the tube size, which is consistent with the XRD findings. Fig. 3(a)–(c) middle panel displays selected area electron diffraction (SEAD) images of the synthesized NTs. The fringes achieved in the SAED image for the ZnO sample indicate the formation of the polycrystalline tetragonal structure of ZnO. It is also essential to note that the broad XRD peak of Gd and Co-doped ZnO suggests small crystallite size and, consequently, a significant surface area. It is evident from the TEM micrograph that the size of Gd–Co co-doped ZnO is greater than that of pure ZnO, implying that the surface area of Gd–Co co-doped ZnO is greater than that of pure ZnO. A larger surface area of the sample is required for enhanced photodegradation efficiency.

Fig. 4 depicts the pure FT-IR, the pure, 0 wt%, 1 wt%, 3 wt%, and 4 wt% Co-doped ZnO NTs. All samples had predominant absorption bands at 3507, 1650, 1115, 995, 788, and 614 cm^{-1}. The absorption spectra at 614 cm^{-1} corresponds to the Zn–O range. The absorbent band at 3507 cm^{-1} corresponds to the OH vibration of water. The band around 1650 cm^{-1} is caused by C=O stretching. Band of absorption detected at 2350 cm^{-1} resembles CO_2 molecules in the air. In contrast, the absorption band at around 995 cm^{-1} indicates the shoulder of resonance interaction between modes of pulsation of oxide ions in nano-crystals with asymmetric stretching. The bands that occur at around 788 cm^{-1} and 1115 cm^{-1} are due to the stretching of Zn–O–Zn and C–O. The band at 3507 cm^{-1} in the FTIR spectrum of the Co-doped ZnO sample corresponds to the –OH mode in H_2O molecules. The presence of these manufactured NPs can be attributed to the atmospheric absorption of water molecules. The 995 cm^{-1} band consists of a shoulder with unequal stretching resonance contact between the vibrational modes of oxide ions in nano-crystals. The ZnO surface quickly absorbs the acetate and hydroxyl assemblies by drying them at temperatures exceeding 600 °C, consistent with the XRD output result, the FTIR result demonstrates that Co occupies the Zn site in the ZnO grid, as the zero peak in the spectrum is identical to that of Co.

All samples were investigated for their optical properties using UV-vis spectroscopy, as shown in Fig. 5. Fig. 5(a) depicts the UV-vis absorption spectra of ZnO and $Zn_{0.96-x}Gd_{0.04}Co_xO$ (Co = 0.01, 0.03, and 0.04) NTs at room temperature and within the wavelength range of 300–900 nm. Compared to ZnO NTs, $Zn_{0.96-x}Gd_{0.04}Co_xO$ (Co = 0.01, 0.03, 0.04) NTs exhibit prominent visible absorption peaks. As the concentration of dopant increases, the absorption peaks of ZnO and $Zn_{0.96-x}Gd_{0.04}Co_xO$ (Co = 0.01, 0.03, and 0.04) shift to wavelengths 370, 380–410 nm. The redshift in the absorption peaks suggests that the sizes of NTs enhance as the concentration of dopant rises. The mean crystallinity rises as a result of disorder and impurities introduced into the ZnO crystal structure by the dopant.[32–35] Using ellipsometry and optical analysis, the electronic transitions of dopant ions were analysed over a broad spectral range (380–410 nm).[31,36] In samples, the electronic transition occurred due to the presence of dopant ions (Gd^{3+} and Co^{2+}) in a tetrahedral.[37–40] Through the wurtzite structure ($P6_3/mmc$ space group) of ZnO, tetrahedrally coordinated O^{2-} and Zn^{2+} ions are formed. Dopant ions (Gd^{3+} and Co^{2+}) replace host ions

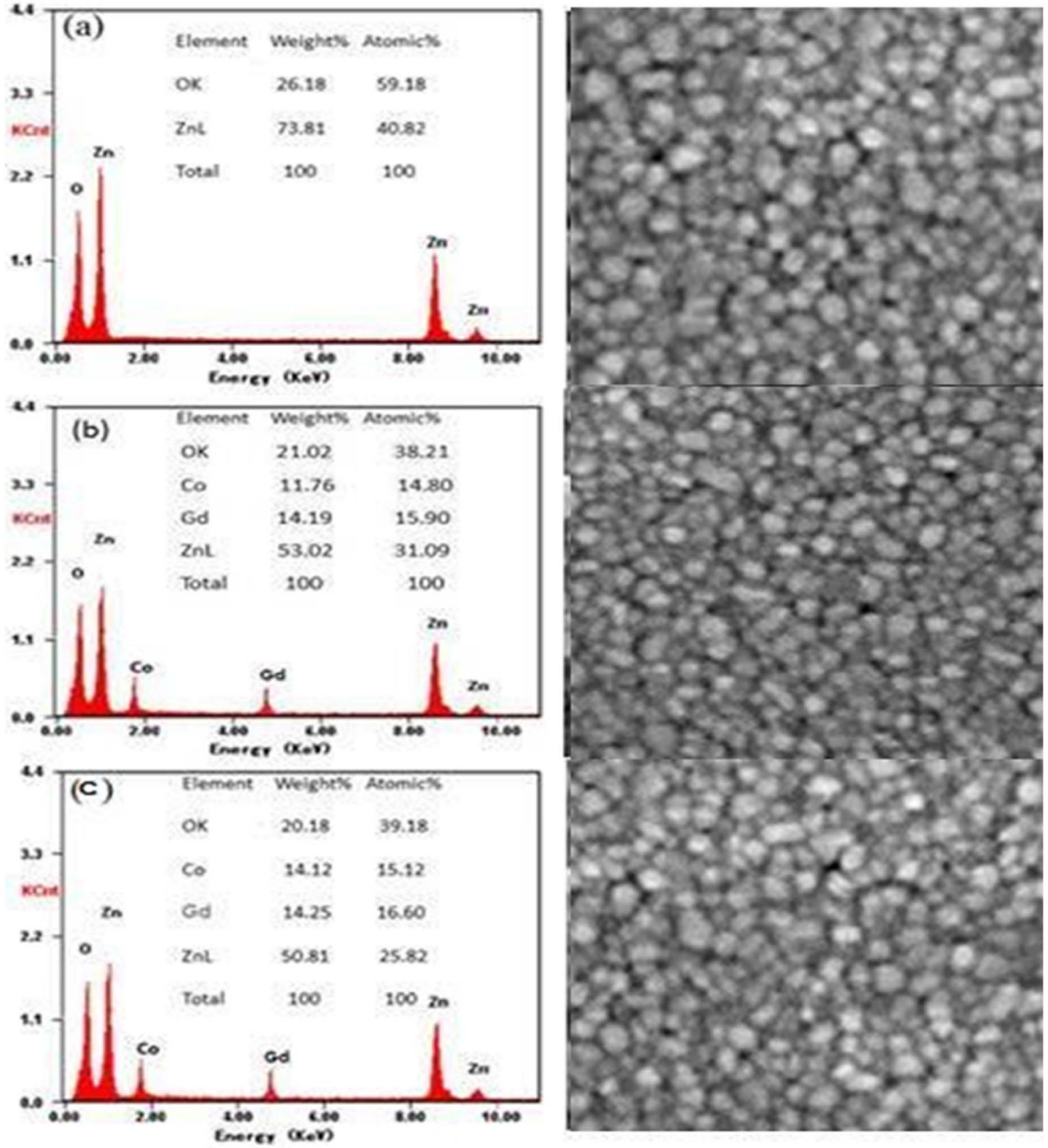

Fig. 2 EDX images of (a) ZnO, (b) $Zn_{0.93}Gd_{0.04}Co_{0.03}O$, (c) $Zn_{0.92}Gd_{0.04}Co_{0.04}O$ and their corresponding SEM images.

(Zn^{2+}) in the absorption spectrum of the visible spectrum. Tauc relation was used to calculate the optical band gap (E_g) of ZnO and $Zn_{0.96-x}Gd_{0.04}Co_xO$ (Co = 0.01, 0.03, 0.04).[41]

$$\alpha h\nu = B(h\nu - E_g)^n \quad (1)$$

where α is the coefficient of optical absorption, B is a constant and $h\nu$ is the energy of the incident photon. For ZnO, n is 1/2 because it has direct bandgap. Fig. 5(b)–(e) depicts the extrapolated bandgap curves for ZnO and $Zn_{0.96-x}Gd_{0.04}Co_xO$ (Co = 0.01, 0.03, 0.04) NTs. In Fig. 4(b) shows that the ZnO NTs have 3.43 eV bandgap that is bigger than the bulk. The bandgap of continuously decreases from 3.45 eV to 3.15 eV with increase in doping concentration (Gd = 4% and Co = 1, 3 and 4%) which are shown in Fig. 5(b)–(e).[42,43] Doping decreased the bandgap of ZnO NTs because an exchange transition between the s–d and p–d electronic states occurred. Bylsma *et al.*, provide an explanation for the narrowing of E_g due to the sp–d exchange interaction effect.[44] The decrease in energy band gap is a result of an increase in the surface-to-volume ratio and an increase in the number of defects.[45,46] Redshift enhancement and bandgap reduction indicate the presence of Gd/Co dopant in the ZnO lattice.[47]

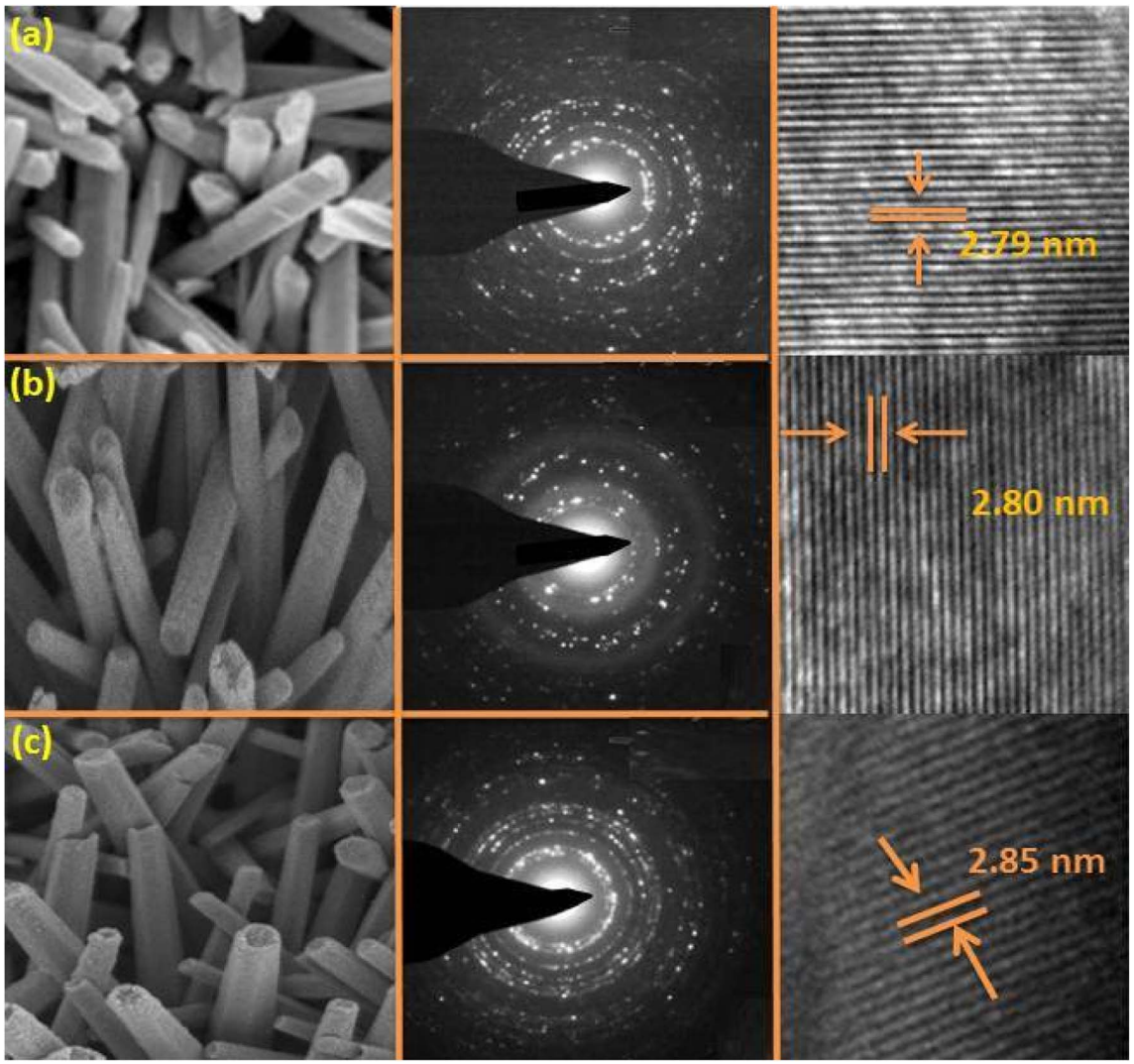

Fig. 3 TEM images of (a) ZnO, (b) $Zn_{0.93}Gd_{0.04}Co_{0.03}O$, (c) $Zn_{0.92}Gd_{0.04}Co_{0.04}O$, their corresponding SEAD images (med panels) and HRTEM micrographs.

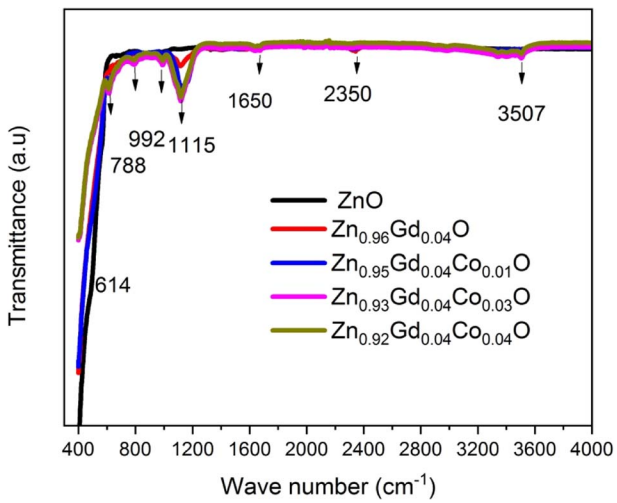

Fig. 4 The FT-IR pattern of pure, 0 wt%, 1 wt%, 3 wt%, and 4 wt% Co-doped ZnO NTs.

3.2 Dielectric properties

3.2.1 Dielectric constant. Fig. 6(a) shows the frequency (f) dependence of dielectric constant (ε_r) for all the specimens annealed at 500 °C. The specimens were prepared by pressing them into circular pellets of 8 mm diameter using a presser before measuring their capacitance, dielectric loss, and a.c. conductivity. The capacitance was measured using gold glue electrodes following the approach used in ref. 3 and 33. The below relation was used to determine the ε_r

$$\varepsilon_r = Cd/\varepsilon_0 A \quad (2)$$

where C represents capacitance, d represents the height of the cylinder, A is the pellet cross-sectional area.

The ε_r values for all samples decrease uniformly with increasing f from 1.5×10^4 Hz and remain constant at higher frequencies. Usually, there are two types of polarizations *i.e.* space charge polarization (SCP) and rotation dielectric polarization (RDP) are responsible for large values of dielectric

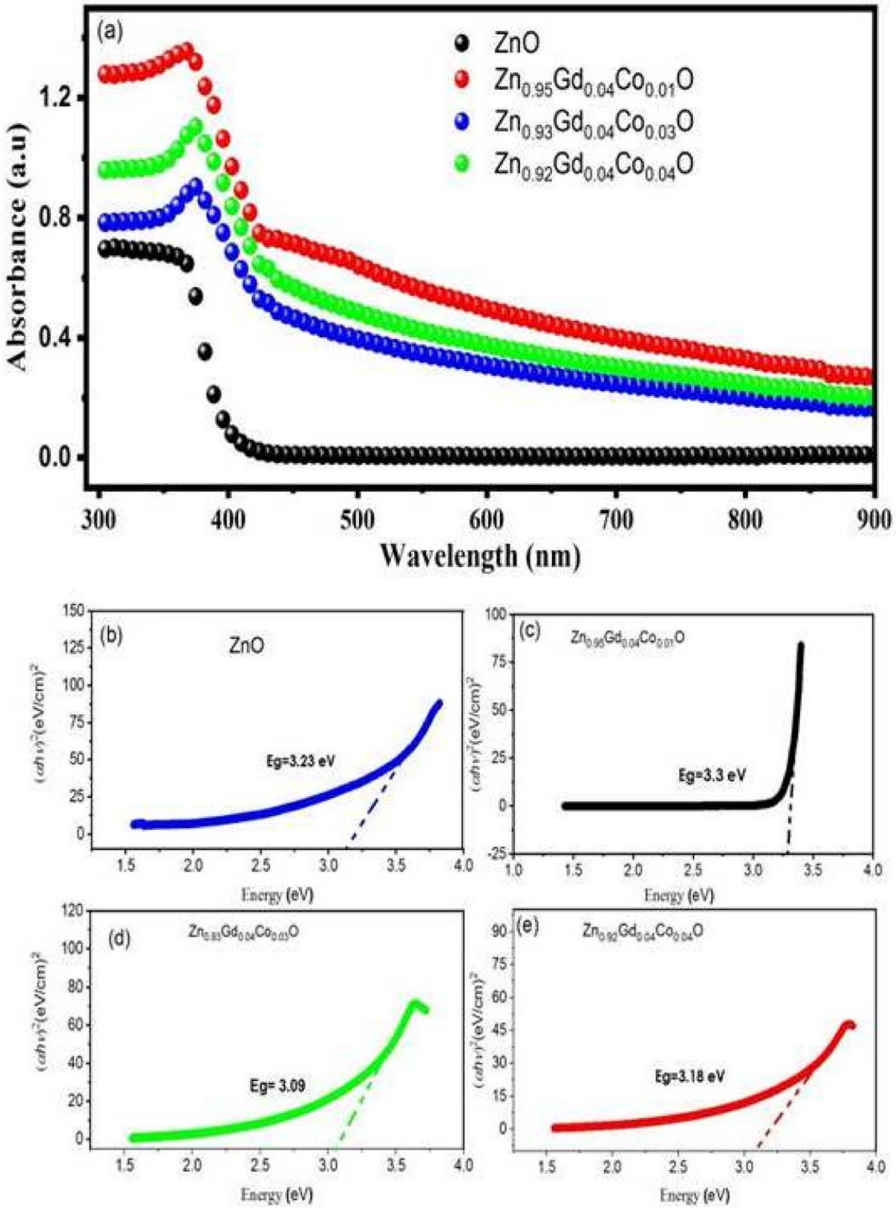

Fig. 5 (a) UV-vis spectroscopy ZnO, and $Zn_{0.96-x}Gd_{0.04}Co_xO$ (Co = 0.01, 0.03, 0.04) NTs. (b)–(e) Calculation of energy band gap using Tauc's plot method for all samples of ZnO, and $Zn_{0.96-x}Gd_{0.04}Co_xO$ (Co = 0.01, 0.03, 0.04).

constants observed. The interfacial region contains many defects like dangling bonds, oxygen vacancies (O_{VS}) and vacancy clusters, *etc.*, where oxygen vacancies can be ionized into single or double ionized vacancies.[29,31]

There will be a large amount of dipole moment (random in direction) generated due to the presence of positive and negative vacancies and the presence of an external magnetic field can only polarize them to induce RDP. Interfacial defects in these nanocrystalline materials will also trap space charge migrating opposite to the electric fields[38,48] thereby inducing SCP and enhanced dielectric constant. This causes grain boundaries to be electrically active. The observed decrease in ε_r with increasing (f) is due to the fact that any species contributing to polarizability is bound to lag behind the applied field. The interfacial area also increases when particles become small and this increases the SCP and RDP whilst Co co-doping enhances the O_{VS} to enhance SCP and RDP. Thus, both crystallize size and doping concentration affect dielectric properties. The ε_r increases with an increase in Co co-doping concentration as shown in Fig. 5(a) and (d) and this emanates from the lattice distortion when small-sized Co^{2+} ions substitute Zn^{2+} ions as previously reported in ref. 26.

3.2.2 Dielectric loss. Fig. 6(b) displays the changes in dielectric loss (ε'') with the (f) of the doped and co-doped ZnO nanoparticles. Here, it is observed that enhancing the frequency, ε'' decreased. Similar behaviour was observed in all the specimens *i.e.* dispersion at low (f) and (f) independence at high frequency. The decrease in ε'' observed at high frequencies

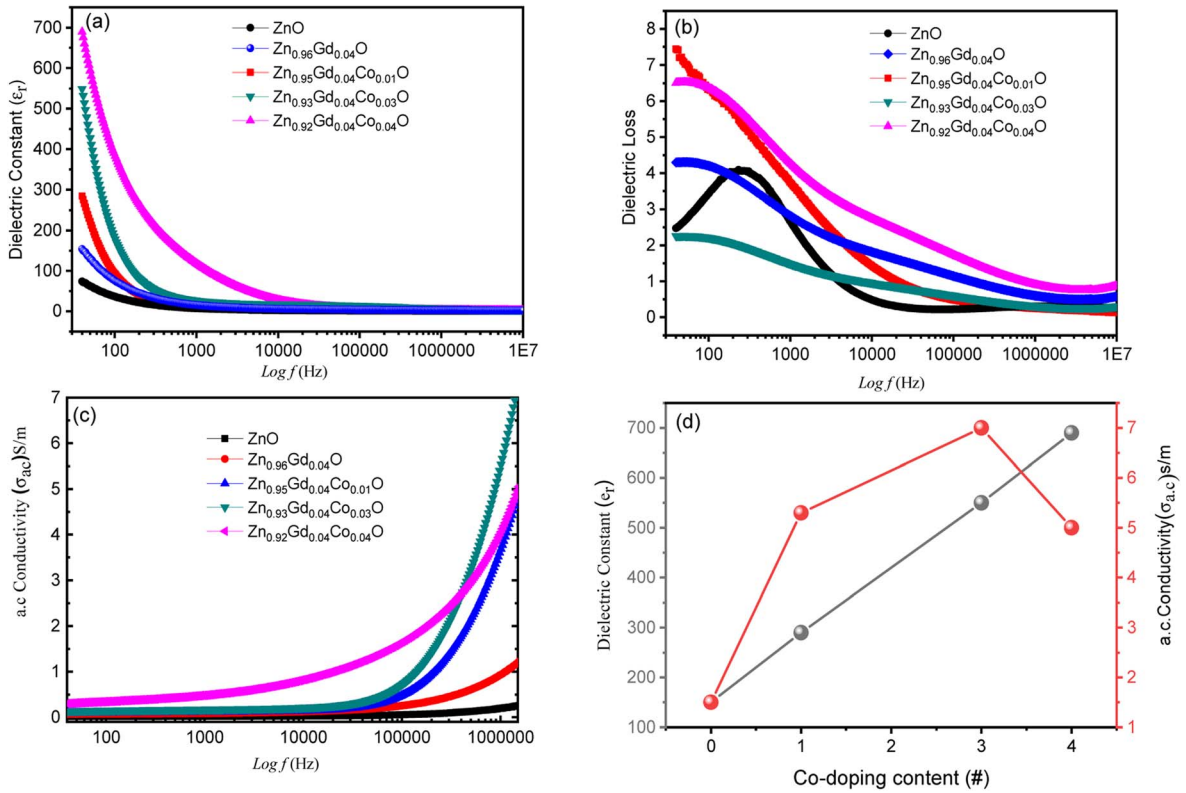

Fig. 6 (a) Variation of ε_r *versus* (*f*) (b) the *f* dependence of ε'' curves, (c) the variation of $\alpha_{a.c.}$with (*f*) curves and (d) phase diagram of dielectric constant and conductivity of pure and Gd doped ZnO and (Gd (fixed), Co)–ZnO co-doped with 4% Gd and Co = 1, 3 and 4%.

is due to ionic migration. The (ε'') found at low and intermediate frequencies (fs) is also attributable to ionic hopping and conduction losses induced by charge transport. Ionic polarisation losses can contribute to this phenomenon. However, at high (fs), ion vibrations might be the only reason.

3.2.3 Electrical conductivity. Fig. 6(c) illustrates the (*f*) AC conductivity ($\alpha_{a.c.}$), AC, of (Gd, Co) co-doped ZnO samples. The $\sigma_{a.c.}$ rises with (*f*) at each voltage and these results are consistent with those reported before.[49] Thus, initially, $\sigma_{a.c.}$ rises slowly with an increase in *f*, whilst at higher frequencies, conductivity sharply increases. Such behaviour is caused by the hopping concept; at low frequency, the $\sigma_{a.c.}$ is constant even though charge carriers travel along infinite pathways, whereas transport is through hopping of charge carriers for *f*-dependent $\sigma_{a.c.}$. For all specimens, $\sigma_{a.c.}$ follows the below relationship

$$\alpha_{a.c.} = \varepsilon_0 \varepsilon'' \omega \quad (3)$$

where $\alpha_{a.c.}$ is the a.c. electrical conductivity, ε'' is the imaginary, ε_r is the dielectric constant of free space, part of the dielectric constant, and $\omega = 2\pi f$, *f* is the frequency. Eqn (2) displays that $\alpha_{a.c.}$ only depends on the ε''. Thus, the ε'' decreases with an increase in *f*, whilst $\alpha_{a.c.}$ enhances. This result corroborates well with previous results, where it was shown that $\alpha_{a.c.}$ increases with an enhancement in (*f*) due to the series resistance effect.[50] There are two possible mechanisms responsible for this behaviour and these are (1) promotion of jumping of charge carriers by electric energy related to the high (*f*) and (2) enhanced dielectric relaxation of ZnO NTs polarization in the high (*f*) region. Thus, co-doped ZnO nanopowder is an excellent material for high-energy storage devices. Moreover, enhanced $\sigma_{a.c.}$ observed may be useful for industrial gas sensing applications due to enhanced electron transmission.[51,52] Fig. 6(d) showed the phase diagram of the dielectric constant and conductivity *versus* doping. It showed that the dielectric behaviour and conductivity increases with doping (as shown in Fig. 5(c) and (d)) because the number of free electrons increases with the addition of impurity ions, which will further help in conduction.

3.3 Magnetic properties

Fig. 7(a) depicts magnetic hysteresis (*M–H*) loops of (Gd, Co) co-doped ZnO NTs recorded at ambient temperature. For pure ZnO, the *M–H* loop shows diamagnetism at 300 K [its data is not shown here] whilst $Zn_{0.96}Gd_{0.04}O$ and $Zn_{0.96-x}Gd_{0.04}Co_xO$ (Co = 0, 0.01, 0.03, 0.04) samples demonstrate an obvious ferromagnetic (FM) response. Fig. 7(a) and (b) shows that for $Zn_{0.96-x}Gd_{0.04}Co_xO$ (Co = 0, 0.01, 0.03, 0.04) specimens, the remanent magnetization (M_r) values are ~0.3367 emu g^{-1}, 0.4413 emu g^{-1}, 0.5788 emu g^{-1}, 0.4538 emu g^{-1} along with coercive field are 47 Oe, 65 Oe, 76 Oe, 49 Oe, respectively. The situation magnetization values 0.52, 1.97, 2.67 and 1.52 ($\times 10^{-2}$ emu g^{-1}) values are listed in Table 2. The table shows that the M_r value of $Zn_{0.92}Gd_{0.04}Co_{0.04}O$ specimen is higher than the literature.[23]

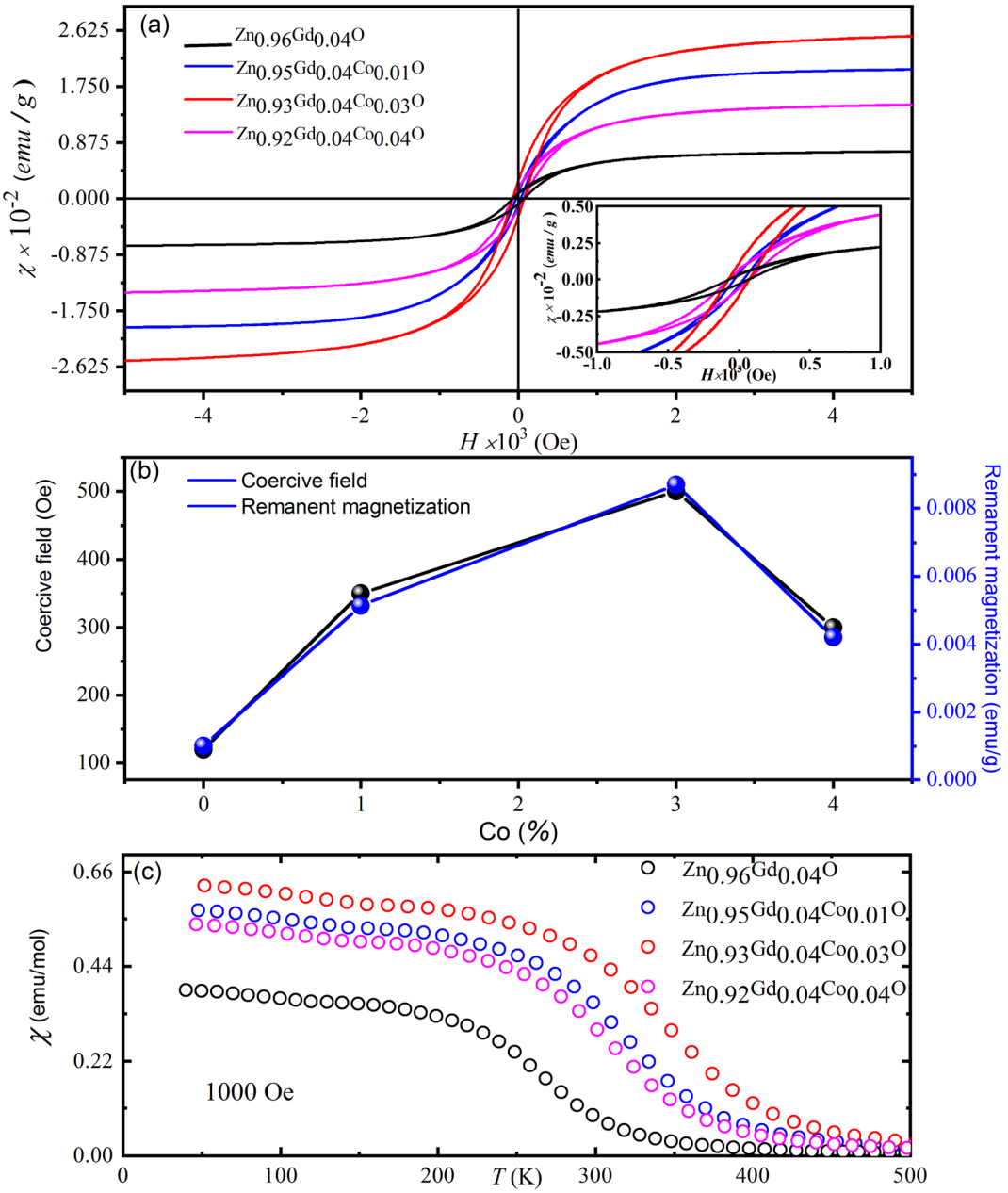

Fig. 7 (a) The magnetic hysteresis (M–H) loops of the (Gd, Co) co-doped ZnO NTs and (b) their corresponding temperature-dependent magnetization and (c) the magnetization *versus* temperature curves for all the doped ZnO NTS.

The transition from paramagnetic to FM states is evident in Fig. 7. M_r values of $Zn_{0.96-x}Gd_{0.04}Co_xO$ (Co = 0.03) specimens are larger than that of pure ZnO. This is due to the fact that O_2 annealing can increase the doping level of Gd and Co ions within the host lattice, hence increasing the number of defects. The RTFM in the 1% Co co-doped specimen may be emanating from intrinsic and extrinsic magnetism sources. Extrinsic sources involve the formation of clusters of transition elements or secondary phases while intrinsic sources involve exchange interactions.

To further explain the magnetic behavior, plots of magnetization with temperature under a magnetic field of 10^3 Oe are displayed in the Fig. 7(c). These data show that $Zn_{0.96-x}Gd_{0.04}Co_xO$ (Co = 0.03) samples have higher FM behavior than either pure Gd or higher Co co-doped specimens. The origins of FM in TM-ZnO[51,52] were shown to be due to coupling between TM ions and bound polarons to form bound magnetic polarons. According to the research of defect-bound transporters for point defect hybridization, TM-doped produces RTFM in doped ZnO. In this study, we show that O_2 annealing can enhance the substitution of Gd and Co into the ZnO lattice. RTFM in $Zn_{0.96-x}Gd_{0.04}Co_xO$ NTs are caused by doping of Gd^{3+} and Co^{2+} for Zn^{2+} and O_2 during annealing to produce O_2 vacancies for maintaining charge balance. This is an interesting novel phenomenon introduced during the specimen preparation process.

Table 2 The magnetic parameters of (Gd, Co) co-doped ZnO magnetic NTs

Sample	Remanent magnetization (M_r) ($\times 10^{-2}$ emu g^{-1})	Coercive field (Oe)	Saturation magnetization (M_s) ($\times 10^{-2}$ emu g^{-1})
$Zn_{0.96}Gd_{0.04}O$	0.3367	50	0.52
$Zn_{0.96}Gd_{0.04}Co_{0.01}O$	0.4413	68	1.97
$Zn_{0.93}Gd_{0.04}Co_{0.03}O$	0.5788	83	2.67
$Zn_{0.92}Gd_{0.04}Co_{0.04}O$	0.4538	53	1.52

As displayed in Fig. 7(c), the lower around 350 K T_C is visible in the $\chi(T)$ Co = 0.03. The displayed decrease in the magnetic moment for Co with higher depends may be related to Co co-doped ZnO specimens' structural property. The changes in cell parameters indicate that lattice constants, and consequently unit cell volume, raise as cobalt concentration rises. The expansion of the unit cell volume increases the distance between the nearest cobalt ions in the ZnO matrix, and this results in antiferromagnetic super-exchange interactions between adjacent Co ions, thereby an increase in magnetic moment. The effect of temperature on the nanoparticles' inverse magnetic susceptibility between 2 and 300 K. It is seen that the inverse susceptibility goes down in a straight line until 380 K, when it drops off the Curie–Weiss line. The modified Curie–Weiss expression fits well with the susceptibility of the nanoparticles we used in our experiments as mentioned below,

$$\chi(T) = \chi_o + (1/8)\mu_{eff}^2 x/(T - \theta_C)$$

where χ_o represents the temperature-independent susceptibility, C the Curie constant and θ_C is the Curie–Weiss temperature, x is the concentration of Co ions and μ_{eff} is the effective moment. The calculated Curie–Weiss law parameters *i.e.*, effective moment μ_{eff} = 2.45 μ_B and $\theta = -25$ K. In contrast, values for replaced $Zn_{0.96-x}Gd_{0.04}Co_xO$ (x = 0.0, 0.1, 0.3, and 0.4) samples are found to decrease with increasing Co co-doped concentration x, with effective moment values ranging between 2.46 and 2.49 μ_B, provide information's related with the exchange integral j, which is a measure of the interaction between the magnetic ions. The negative values of suggest that the magnetic dopants have a relatively weak antiferromagnetic interaction.[53,54] Most other oxide compounds have a value between 24 and 27 K, which is virtually as low as the value for Co-doped ZnO. Most other oxide compounds have a value between 24 and 27 K, which is virtually as low as the value for Co-doped ZnO. The magnetic properties found at low temperatures may result from flaws introduced during manufacturing or the existence of impurity phases. Clarification of this aspect requires further research.

4. Conclusions

ZnO and ferromagnetic (Gd, Co) co-doped ZnO NTs were successfully fabricated in this work. XRD measurements show that all the (Gd, Co) co-doped specimens have a tetragonal structure. With an increase in either (f) or Co dopant concentration, both dielectric constant and dielectric loss and electrical conductivity increases. The electrical conductivity of annealed Gd and Co-doped ZnO specimens was found to be enhanced. This occurred as a result of the substitution of Zn ions with Gd and Co ions, which increased the number of available charge carriers. A significant change in the hysteresis loop was observed, characterized by the change from the diamagnetic behavior of ZnO to ferromagnetic when co-doped with (Gd, Co). The enhanced dielectric and magnetic responses of the specimens are strongly correlated to an increase in O_2 vacancies and zinc interstitials. Our results indicate that ferromagnetism in the ZnO NTs can be introduced through Gd fixed and limited Co doping and annealing at 500 °C due to the production of extra charge carriers and O_2 vacancies.

Data availability

The datasets generated during and/or analyzed during the current study are available from the corresponding author upon reasonable request. Also, the manuscript's experimental work and wording is original. No part of the was manuscript found plagiarized. If the reviewer further needs the proof then we will send the plagiarized proof.

Author contributions

Rajwali Khan, Ihab Shigidi, Sattam Al Otaibi, Khaled Althubeiti, Nasir Rahman, Mohammad Sohail, Alamzeb Khan, Shahid Iqbal, Tommaso Del Rosso, Quaid Zaman, Aurangzeb Khan write this paper with their mutual discussion. Aurangzeb Khan and Rajwali Khan, created the idea and submitted the paper.

Funding

The authors extend their appreciation to the Deanship of Scientific Research at King Khalid University for funding this work through Small Groups Project under grant number RGP.1/25/43.

Conflicts of interest

The authors declare that they have no known competing financial interests or personal relationships that could have influenced the work reported in this paper.

Acknowledgements

The authors acknowledge the financial support from King Khalid University for sponsorship and support. We also acknowledge the support and guidance provided by King Khalid University.

References

1 Y. Hao, *et al.*, Novel magnetic behavior of Mn-doped ZnO hierarchical hollow spheres, *J. Nanopart. Res.*, 2012, **14**(1), 1–9.
2 G. A. Prinz, Magnetoelectronics, *Science*, 1998, **282**(5394), 1660–1663.
3 R. Khan, *et al.*, Structure and magnetic properties of (Co, Ce) co-doped ZnO-based diluted magnetic semiconductor nanoparticles, *J. Mater. Sci.: Mater. Electron.*, 2021, **32**(19), 24394–24400.
4 P. Li, *et al.*, Structural and optical properties of Co-doped ZnO nanocrystallites prepared by a one-step solution route, *J. Lumin.*, 2012, **132**(1), 220–225.
5 R. Khan, *et al.*, Effect of Sn-doping on the structural, optical, dielectric and magnetic properties of ZnO nanoparticles for spintronics applications, *J. Mater. Sci.: Mater. Electron.*, 2021, **32**(16), 21631–21642.
6 X. Wang, *et al.*, Properties of Ni doped and Ni–Ga co-doped ZnO thin films prepared by pulsed laser deposition, *J. Alloys Compd.*, 2011, **509**(7), 3282–3285.
7 Y.-M. Hao, *et al.*, Structural, optical, and magnetic studies of manganese-doped zinc oxide hierarchical microspheres by self-assembly of nanoparticles, *Nanoscale Res. Lett.*, 2012, **7**(1), 1–9.
8 A. Stroppa, X. Duan and M. Peressi, Structural and magnetic properties of Mn-doped GaAs(1 1 0) surface, *Mater. Sci. Eng. B*, 2006, **126**(2–3), 217–221.
9 Y. Chang, *et al.*, Synthesis, optical, and magnetic properties of diluted magnetic semiconductor $Zn_{1-x}Mn_xO$ nanowires via vapor phase growth, *Appl. Phys. Lett.*, 2003, **83**(19), 4020–4022.
10 Y. Ohno, *et al.*, Electrical spin injection in a ferromagnetic semiconductor heterostructure, *Nature*, 1999, **402**(6763), 790–792.
11 L. Sun, *et al.*, Room-temperature ferromagnetism and in-plane magnetic anisotropy characteristics of nonpolar GaN:Mn films, *Appl. Surf. Sci.*, 2009, **255**(16), 7451–7454.
12 T. Dietl, A ten-year perspective on dilute magnetic semiconductors and oxides, *Nat. Mater.*, 2010, **9**(12), 965–974.
13 X. Xu and C. Cao, Structure and ferromagnetic properties of Co-doped ZnO powders, *J. Magn. Magn. Mater.*, 2009, **321**(14), 2216–2219.
14 C. F. Klingshirn, Optical properties of bound and localized excitons and of defect states, in *Semiconductor Optics*, 2012, Springer, pp. 363–382.
15 Q. Wang, Q. Sun and P. Jena, Ab initio study of electronic and magnetic properties of the C-codoped $Ga_{1-x}Mn_xN$ $(10\bar{1}0)$ surface, *Phys. Rev. B: Condens. Matter Mater. Phys.*, 2007, **75**(3), 035322.
16 J. Fu, *et al.*, Synthesis and structural characterization of ZnO doped with Co, *J. Alloys Compd.*, 2013, **558**, 212–221.
17 N. G. Szwacki, J. Majewski and T. Dietl, Aggregation and magnetism of Cr, Mn, and Fe cations in GaN, *Phys. Rev. B: Condens. Matter Mater. Phys.*, 2011, **83**(18), 184417.
18 Z. Lu, *et al.*, Carrier-mediated ferromagnetism in single crystalline (Co, Ga)-codoped ZnO films, *Appl. Phys. Lett.*, 2009, **94**(15), 152507.
19 G. Husnain, F. Tao and S.-D. Yao, Structural and magnetic properties of Co+ implanted n-GaN dilute magnetic semiconductors, *Phys. B*, 2010, **405**(9), 2340–2343.
20 V. Gandhi, *et al.*, Effect of cobalt doping on structural, optical, and magnetic properties of ZnO nanoparticles synthesized by coprecipitation method, *J. Phys. Chem. C*, 2014, **118**(18), 9715–9725.
21 H. Hao, M. Qin and P. Li, Structural, optical, and magnetic properties of Co-doped ZnO nanorods fabricated by a facile solution route, *J. Alloys Compd.*, 2012, **515**, 143–148.
22 T. Oshio, *et al.*, Effect of Mn doping on the electric and dielectric properties of ZnO epitaxial films, *J. Appl. Phys.*, 2008, **103**(9), 093717.
23 R. Khan, M.-U. Rahman and S. Fashu, Effect of annealing temperature on the dielectric and magnetic response of (Co, Zn) co-doped SnO_2 nanoparticles, *J. Mater. Sci.: Mater. Electron.*, 2017, **28**(3), 2673–2679.
24 A. Yu, *et al.*, Micro-lotus constructed by Fe-doped ZnO hierarchically porous nanosheets: preparation, characterization and gas sensing property, *Sens. Actuators, B*, 2011, **158**(1), 9–16.
25 R. Khan and Y. Zaman, Effect of annealing on structural, dielectric, transport and magnetic properties of (Zn, Co) co-doped SnO_2 nanoparticles, *J. Mater. Sci.: Mater. Electron.*, 2016, **27**(4), 4003–4010.
26 R. Khan, S. Fashu and M.-U. Rahman, Effects of Ni co-doping concentrations on dielectric and magnetic properties of (Co, Ni) co-doped SnO_2 nanoparticles, *J. Mater. Sci.: Mater. Electron.*, 2016, **27**(8), 7725–7730.
27 R. Khan and S. Fashu, Effect of annealing on Ni-doped ZnO nanoparticles synthesized by the co-precipitation method, *J. Mater. Sci.: Mater. Electron.*, 2017, **28**(14), 10122–10130.
28 C. Cong, *et al.*, Effects of temperature on the ferromagnetism of Mn-doped ZnO nanoparticles and Mn-related Raman vibration, *Nanotechnology*, 2006, **17**(5), 1520.
29 R. Khan, S. Fashu and Y. Zaman, Magnetic and dielectric properties of (Co, Zn) co-doped SnO_2 diluted magnetic semiconducting nanoparticles, *J. Mater. Sci.: Mater. Electron.*, 2016, **27**(6), 5960–5966.
30 T. Castro, *et al.*, Size controlling and tailoring the properties of $Gd_xZn_{1-x}O$ nanoparticles, *Ceram. Int.*, 2022, **48**(3), 4324–4331.
31 R. Khan, *et al.*, Structure and magnetic properties of (Co, Mn) co-doped ZnO diluted magnetic semiconductor nanoparticles, *J. Mater. Sci.: Mater. Electron.*, 2018, **29**(1), 32–37.

32 K. Rajwali and M.-H. Fang, Dielectric and magnetic properties of (Zn, Co) co-doped SnO_2 nanoparticles, *Chin. Phys. B*, 2015, **24**(12), 127803.
33 R. Khan, *et al.*, Effect of air annealing on the structure, dielectric and magnetic properties of (Co, Ni) co-doped SnO_2 nanoparticles, *J. Mater. Sci.: Mater. Electron.*, 2016, **27**(10), 10532–10540.
34 P. Jongnavakit, *et al.*, Preparation and photocatalytic activity of Cu-doped ZnO thin films prepared by the sol–gel method, *Appl. Surf. Sci.*, 2012, **258**(20), 8192–8198.
35 W.-J. Qin, *et al.*, Control of Cu-doping and optical properties of ZnO quantum dots by laser ablation of composite targets, *Mater. Chem. Phys.*, 2011, **130**(1–2), 425–430.
36 K. J. Kim and Y. R. Park, Optical absorption and electronic structure of $Zn_{1-x}Mn_xO$ alloys studied by spectroscopic ellipsometry, *J. Appl. Phys.*, 2003, **94**(2), 867–869.
37 J. Han, *et al.*, Optical and dielectric properties of ZnO tetrapod structures at terahertz frequencies, *Appl. Phys. Lett.*, 2006, **89**(3), 031107.
38 F. Gu, *et al.*, Photoluminescence properties of SnO_2 nanoparticles synthesized by sol–gel method, *J. Phys. Chem. B*, 2004, **108**(24), 8119–8123.
39 S. Deka and P. Joy, Synthesis and magnetic properties of Mn doped ZnO nanowires, *Solid State Commun.*, 2007, **142**(4), 190–194.
40 M. Patra, *et al.*, Studies on structural and magnetic properties of Co-doped pyramidal ZnO nanorods synthesized by solution growth technique, *J. Phys. Chem. Solids*, 2009, **70**(3–4), 659–664.
41 K. Safeen, *et al.*, Synthesis of Nb-doped TiO_2 films on rigid and flexible substrates at low temperature, *Mod. Phys. Lett. B*, 2019, **33**(26), 1950313.
42 M. Ahmad, *et al.*, Preparation of highly efficient Al-doped ZnO photocatalyst by combustion synthesis, *Curr. Appl. Phys.*, 2013, **13**(4), 697–704.
43 C. Belkhaoui, *et al.*, Enhancing the structural, optical and electrical properties of ZnO nanopowders through (Al+Mn) doping, *Results Phys.*, 2019, **12**, 1686–1696.
44 R. Bylsma, *et al.*, Dependence of energy gap on x and T in $Zn_{1-x}Mn_xSe$: the role of exchange interaction, *Phys. Rev. B: Condens. Matter Mater. Phys.*, 1986, **33**(12), 8207.
45 A. Layek, B. Manna and A. Chowdhury, Carrier recombination dynamics through defect states of ZnO nanocrystals: from nanoparticles to nanorods, *Chem. Phys. Lett.*, 2012, **539**, 133–138.
46 C. Mrabet, *et al.*, Some physical investigations on hexagonal-shaped nanorods of lanthanum-doped ZnO, *J. Alloys Compd.*, 2015, **648**, 826–837.
47 E. Pragna, *et al.*, Nano Synthesis and Characterization of Co and Mn Co-Doped ZnO by Solution Combustion Technique, *J. Supercond. Novel Magn.*, 2021, 1–10.
48 S.-P. Szu and C.-Y. Lin, AC impedance studies of copper doped silica glass, *Mater. Chem. Phys.*, 2003, **82**(2), 295–300.
49 O. Pakma, *et al.*, Influence of frequency and bias voltage on dielectric properties and electrical conductivity of $Al/TiO_2/p\text{-}Si/p^+$(MOS) structures, *J. Phys. D: Appl. Phys.*, 2008, **41**(21), 215103.
50 R. Elilarassi and G. Chandrasekaran, Synthesis and characterization of ball milled Fe-doped ZnO diluted magnetic semiconductor, *Optoelectronics Letters*, 2012, **8**(2), 109–112.
51 Y. Lin, *et al.*, Fe-doped ZnO magnetic semiconductor by mechanical alloying, *J. Alloys Compd.*, 2007, **436**(1–2), 30–33.
52 S. Yin, *et al.*, Absence of ferromagnetism in bulk polycrystalline $Zn_{0.9}Co_{0.1}O$, *Phys. Rev. B: Condens. Matter Mater. Phys.*, 2006, **73**(22), 224408.
53 T. Fukumura, *et al.*, Magnetic properties of Mn-doped ZnO, *Appl. Phys. Lett.*, 2001, **78**(7), 958–960.
54 L. Yang, *et al.*, In situ synthesis of Mn-doped ZnO multileg nanostructures and Mn-related Raman vibration, *J. Appl. Phys.*, 2005, **97**(1), 014308.